Journal of Molecular Graphics and Modelling 51 (2014) 79–85

Contents lists available at ScienceDirect

Journal of Molecular Graphics and Modelling

journal homepage: www.elsevier.com/locate/JMGM

The effect of intermolecular interactions on the charge transport properties of thiazole/thiophene-based oligomers with trifluoromethylphenyl

Ling Liu, Guochun Yang*, Xiaodan Tang, Yun Geng, Yong Wu, Zhongmin Su**

Faculty of Chemistry, Institute of Functional Material Chemistry, Northeast Normal University, Changchun, 130024 Jilin, PR China

ARTICLE INFO

Article history:
Accepted 28 April 2014
Available online 5 May 2014

Keywords:
Thiazole
Thiophene
Charge transport
Intermolecular interaction
Band model

ABSTRACT

A fundamental understanding of the relationship between intermolecular interactions and transport properties in organic semiconducting materials is significant for their potential applications as electronic device element. Carrier transport properties of thiazole/thiophene-based oligomers with trifluoromethylphenyl groups **1**, **2**, and **3**, in which the type and strength of the intermolecular interactions are different, were investigated within the framework of band model. The results show that π–π stacking interactions are mainly responsible for the hole transport, while hydrogen bonding interactions have a great influence on the electron transport. The specific transport mechanism could be explained by analyzing the density of states (DOS) and Γ point wave functions.

1. Introduction

Organic semiconducting materials have been widely used as organic electronic devices such as organic light emitting diodes (OLEDs) [1,2], organic field effect transistors (OFETs) [3,4] and organic photovoltaic cells (OPVs) [5], which is due to the reason that these materials offer attractive benefits of low cost, large-area, light weight and flexibility [6,7]. The continued emergence for these applications will mainly depend on performance enhancement of such materials. Thus, the development of organic semiconducting materials has become an active field of research in recent years.

Charge transport ability in organic semiconducting materials is one of the most important properties for the performance of OLEDs, OFETs, and organic solar cells [8]. Organic semiconductors can be generally divided into three types by their charge transporting abilities: hole, electron, and ambipolar transport material. Great efforts in the past have been put into the development of hole transport materials; however, the number of electron transport materials is still quite limited [9–11]. The mobilities of electron transport materials are generally less than those of the hole transport ones. By introducing electron-withdrawing groups such as fluorine [12], carbonyl [13–16], perfluoroalkyl [17–20], and cyano [21–23] substituents into hole-transporting (p-type) π-conjugated systems, we can lower the lowest unoccupied molecular orbital (LUMO) energy level leading to the creation of electron-transporting semiconducting materials, which has accelerated the development of electron transport materials [24]. Ambipolar transport material can transport both electrons and holes alternatively or even simultaneously. This has been demonstrated in many recent experimental studies by means of different approaches and a more detailed description can be found in a recent review [25].

Recently, a series of thiazole/thiophene-based oligomers with trifluoromethylphenyl were synthesized by Yamashita and coworkers. Although these compounds have similar molecular structures with thiazole or thiophene rings in the middle and trifluoromethylphenyl groups on both sides, they exhibit very different charge transport properties. For example, electron mobility of compound **1** and **3** are 0.21 $cm^2 V^{-1} s^{-1}$ and 0.07 $cm^2 V^{-1} s^{-1}$, respectively [26]. Electron mobility of compound **2** is not observed [27]. It should be noted that Yamashita group only measured their electron mobilities. Their molecular and crystal structures were shown in Fig. 1. The molecule 2,2′-bis(4-trifluoromethylphenyl)-5,5′-bithiazole **1** and 5,5′-bis(4-trifluoromethylphenyl)-2,2′-bithiophene **3** are completely planar, while 2,2′-bis(4-trifluoromethylphe nyl)-2,2′-bithiazole **2** has respective torsion angles of 1.6° and 10.4° between the thiazole and 4-trifluoromethylphenyl rings though torsion angle is 0° between the thiazole rings. Thus, these differences in molecular structures lead to different packing motifs in crystals, which contain different interactions. Crystals **1** and **2** contain both hydrogen-bonding

* Corresponding author. Tel.: +86 041385099521.
** Corresponding author.
E-mail address: yanggc468@nenu.edu.cn (G. Yang).

http://dx.doi.org/10.1016/j.jmgm.2014.04.016
1093-3263/

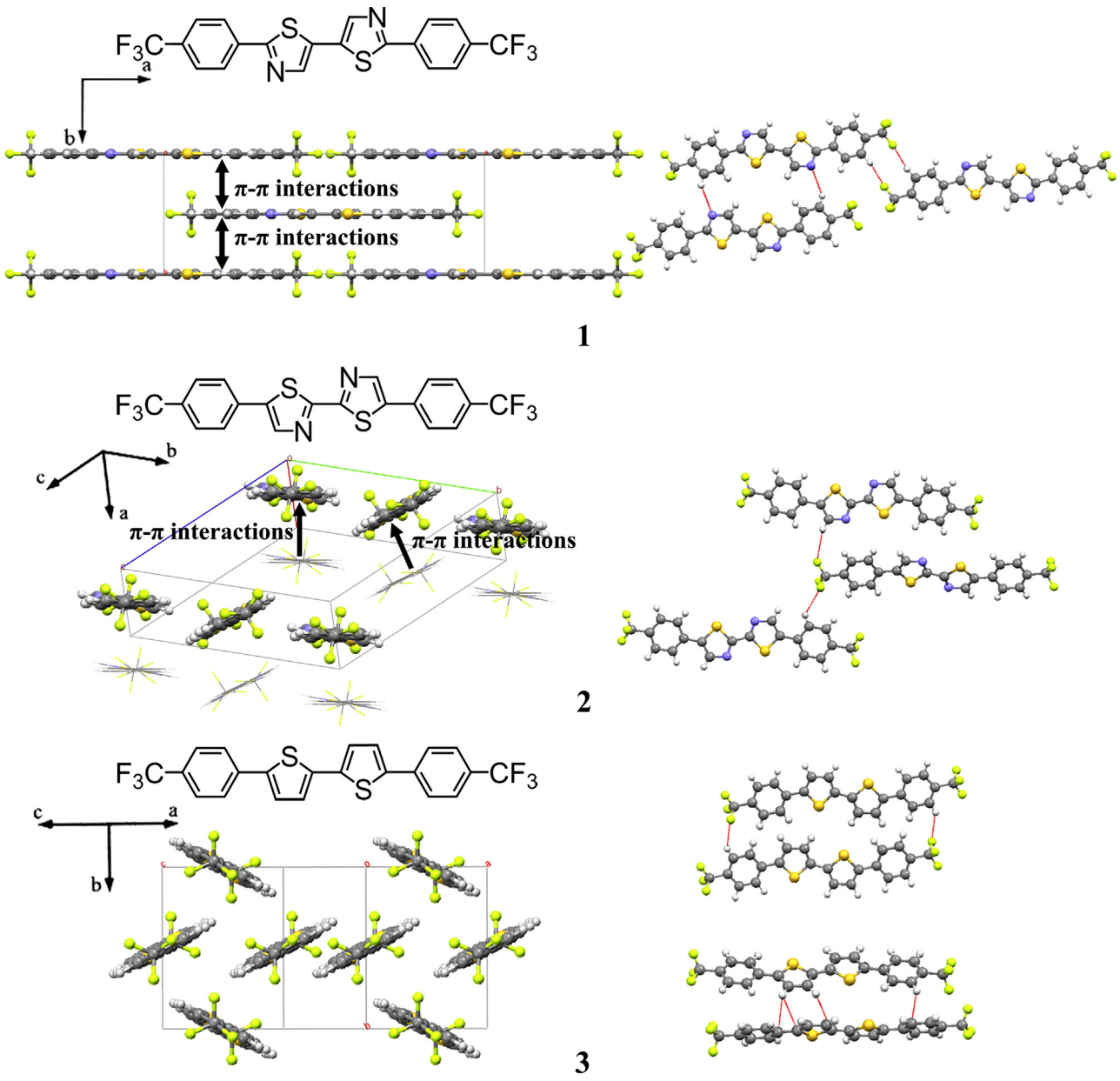

Fig. 1. Molecular structure, crystal structures (left) and potential hydrogen bonds (right) of **1**, **2**, and **3**.

and π–π stacking interactions, while crystal **3** only contains hydrogen-bonding interaction. In this article, with the help of density functional theory calculations, our goal is to shed light on the relationship between intermolecular interactions and charge transport properties.

Now, first principle band structure calculations have been widely applied in the investigation of organic crystals, giving the insights of internal properties from the viewpoint of molecular packing [28–30]. For example, density functional theory (DFT) coupled with band theory was used to discuss the impact of fluorine- and alkyl/alkoxy substituents on oligoacene crystals, and obtained a good understanding of the role of substitution on the charge transporting process [31]. The charge transport properties of oligoacene crystals from naphthalene to pentacene were investigated by using the DFT and molecular mechanics (MM) approaches. The results show that ability of charge transport depends not only on π stacking area but also on the distances between π-stacking [32]. Our group also investigated the charge transport mechanism of a series of organic photoelectric materials [33–35].

2. Theoretical methodology

Generally, there are two models to describe the charge transport mechanism at present: hopping model and band-like model. The charge transport is governed by hopping mechanism when the system is disordered at room temperature. But in the well ordered organic crystals, the mobility is more rationally described by band-like model. Here, a standard band-theory model was used.

When proceeding DFT calculation, the main question becomes whether the local-density approximations (LDA) or the generalized gradient approximation (GGA) should be used. Actually, the LDA uses the first term of a Taylor expansion of the uniform density. The electron gas is considered to be homogeneous, which is not exactly true in the real circumstance. In order to obtain better approximations of the exchange-correlation functional, by extend-

ing the series with the next lowest term, the GGA uses not only the information about the density $\rho(\rightarrow r)$ at a particular point $\rightarrow r$, but supplements the density with information about the gradient of the gradient of the charge density, $\nabla\rho(\rightarrow r)$ is introduced to account for the non-homogeneity of the true electron density. Here, we choose the GGA–PBE because it is frequently used in structure and charge transport property calculations of organic semiconducting materials and usually obtains reasonable results [36–39].

Electronic band structure and density of states (DOS) calculations were performed by a density functional theory (DFT) method implemented in the Vienna Ab-initio Simulation Package (VASP 5.2.12) [40,41] with Perdew–Burke–Emzerhof (PBE) for the exchange correlation functional, a plane-wave basis set with cutoff energy cut-off of 400 eV [42,43] and PAW–PBE potential for each of the elements. For crystal structure **1**, **2**, and **3**, space groups were *C2/m*, *P-1*, *P21/a*, respectively. Also lattice parameters and *k*-grids were $a = 18.58$ Å, $b = 6.736$ Å, $c = 7.380$ Å, $\alpha = \gamma = 90^\circ$, $\beta = 104.7^\circ$, for crystal **1**, $a = 4.688$ Å, $b = 13.37$ Å, $c = 14.57$ Å, $\alpha = 99.62^\circ$, $\beta = 97.97^\circ$, $\gamma = 94.74^\circ$, for crystal **2**, and $a = 6.154$ Å, $b = 7.604$ Å, $c = 19.50$ Å, $\alpha = \gamma = 90^\circ$, $\beta = 97.18^\circ$, for crystal **3**. The *k*-grids were respectively chosen as $3 \times 8 \times 7$, $5 \times 3 \times 3$, and $6 \times 5 \times 2$ for the three crystals as a compromise between accuracy and computational power, using the Monkhorst–Pack scheme to sample the Brillouin zone. The calculated the band structure with and without vdW-DF of these systems using their optimized crystal structures. The selected bond lengths and bond angles along with experimental values are listed in Table S1. The results show that the influence of the optimization on the structure is negligible. The band structures of crystals **1**, **2**, and **3** of experimental crystal structures, optimized crystal structures, and optimized crystal structures with vdW-DF are shown in Fig. S2. The changes of the larger bandwidths (eV) along high symmetry lines of experimental crystal structures optimized crystal structures and optimized crystal structures with vdW-DF is very small (Table S2), which indicate that using the experimental crystal structures to calculate their band structures is reliable. Subsequently, the data calculated using the experimental crystal structures is adopted. Meanwhile, Γ point wave functions calculations were performed though $D\,\mathrm{mol}^3$ within the Material Studio [44,45] package with the generalized gradient approximation (GGA) in Perdew–Burke–Ernzerhof (PBE) form and all-electron double numerical basis set with polarized function (DNP basis set) [46].

3. Results and discussion

3.1. Geometric structure

The molecular and crystal structures of thiazole/thiophene-based oligomers with trifluoromethylphenyl groups **1**, **2**, and **3** were shown in Fig. 1 (left). At the molecular level, the main difference is the existence and position of the nitrogen atom. Furthermore, the 5,5′-bithiazole **1** and bithiophene derivative **3** are completely planar, while 2,2′-bithiazole **2** has torsion angles of 1.6° and 10.4°, respectively, between the thiazole and 4-trifluoromethylphenyl rings though torsion angle is 0° between the thiazole rings.

As we know, the charge transport properties in organic transport materials are closely related to their packing motifs [47]. Fig. 1 (right) shows the crystal structure and potential hydrogen bonds of **1**, **2**, and **3**. Crystal **1** forms a closely packed two-dimensional columnar structure with separation in the direction of the *b*-axis of 3.37 Å between the stacked molecules, which has been known as favorable for π–π interactions while CH–F and CH–N interactions stretch parallel to the *ac* plane with CH–F and CH–N distances being 2.343 Å and 2.667 Å, respectively. As to structure **2**, it forms a herringbone packing with a small torsion angle between two crystallographically independent molecules because of the twisting of the molecule with separation of 3.81 Å between the stacked molecules, which is in the range of π–π interactions. And hydrogen bond CH–F in crystal **2** is in the direction along the *a*-axis, which is same as π–π interactions. For structure **3**, it also has a herringbone packing, while the bithiophene derivative grows separate way in a very big torsion angle between molecules with distance of 3.66 Å between planar molecules. The CH–π interactions in crystal **3** stretch from molecule edge to the surface of other molecule paralleling to the *ab* plane while CH–F interactions in the direction of the *a*-axis.

Table 1
The largest bandwidth in VB and CB of **1** along high symmetry lines in eV.

	VB	CB
ΓY	0.284	0.185
ΓL	0.248	0.270

3.2. Band structure

In general, the appearance of both dispersive and flat bands is a reflection of anisotropy in the charge transport properties of the crystal, and the stronger the dispersion of band is, the larger the carrier mobility is. With the help of first principle calculations, we calculated the band structures of crystal structures **1**, **2**, and **3**. Their electronic band structures along high symmetry directions were shown in Fig. 2. The calculated larger bandwidths in valence band (VB) and conduction band (CB) together with their corresponding directions were listed in Tables 1 and 2, respectively. As we can see, both **1** and **3** are direct semiconductors with band gap of 1.82 eV and 2.03 eV, since their maximum of VB and minimum of CB are the same point. Crystal **2** is an indirect semiconductor with a band gap of 1.91 eV.

From Fig. 2(a), we can see that the VB and CB of crystal **1** are in mirror symmetry, which should perform equal transport properties on both hole and electron. Moreover, the bandwidths of both valence band (VB) and conduction band (CB) along the two directions are almost equal to each other (Table 1). In other words, crystal **1** may have the potential to be used as an ambipolar organic transport material. The largest dispersions for both CB and VB in the first Brillouin zone along high-symmetry directions are $\Gamma \rightarrow Y$ and $\Gamma \rightarrow L$, respectively. Among the two directions with larger bandwidths, $\Gamma \rightarrow Y$ corresponds to the *b*-axis direction in real space, $\Gamma \rightarrow L$ is parallel to the *ac* plane. Thus, the π–π interactions mainly dominate the hole transport, while the hydrogen bonding interactions are responsible for the electron transport.

For crystal **2**, both occupied and unoccupied bands consist of two subbands due to the two translationally inequivalent molecules present in the unit cell (Fig. 2b). The largest bandwidths are along high-symmetry direction $\Gamma \rightarrow X$ only, which corresponds to *a*-axis in the real space. It is interesting to find that the bandwidth (0.445 eV) in valence band (VB) is much larger than that (0.155 eV) in conduction band (CB), which means that hole mobility of crystal **2** is larger than that of electron mobility. Although the hydrogen bonding and π-stacking interactions coexist in crystals **1** and **2**,

Table 2
The largest bandwidth in VB and CB of **3** along high symmetry lines in eV.

	VB	CB
ΓC	–	0.186
ΓY	–	0.189

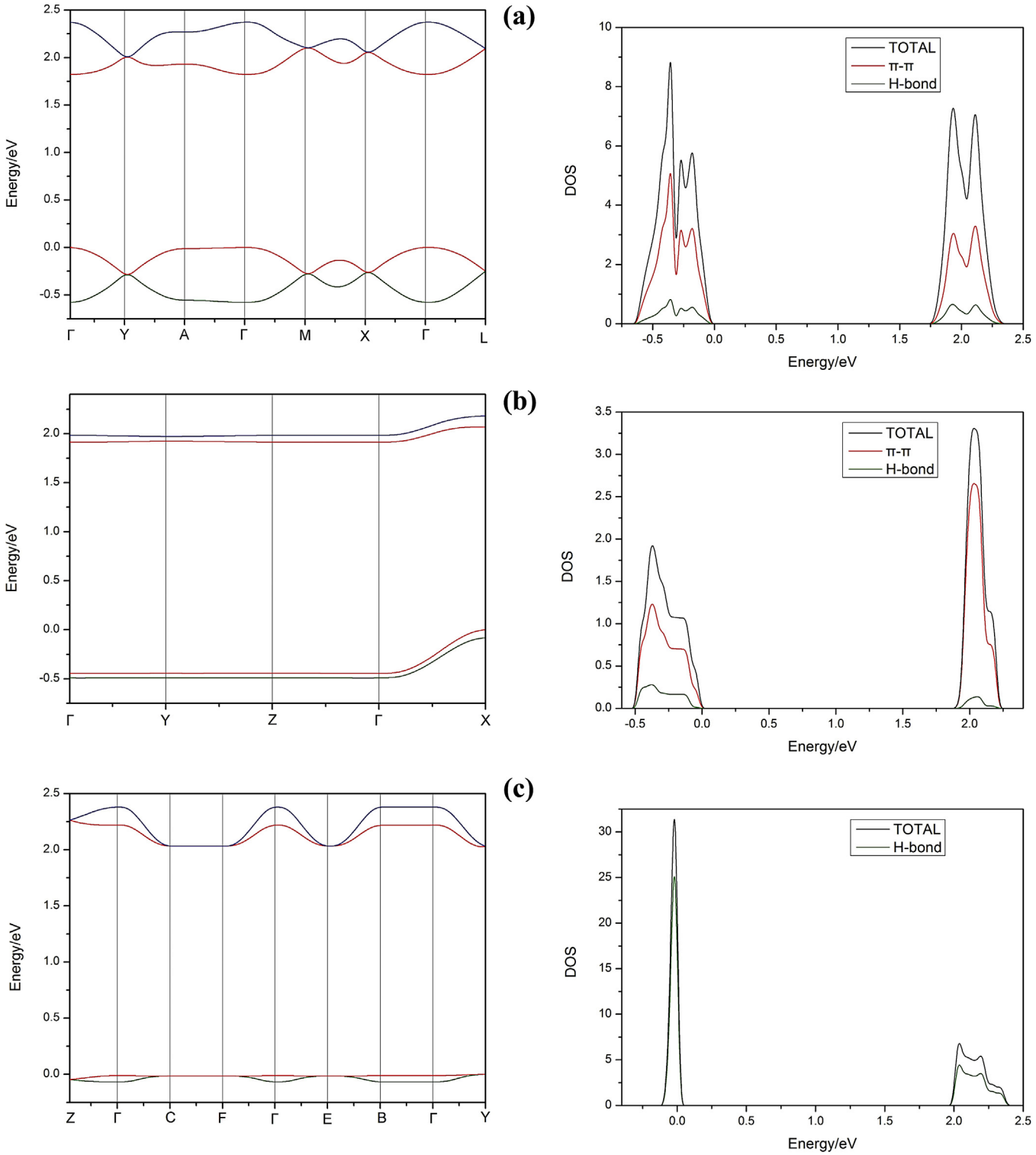

Fig. 2. Band structures (left) and DOS (right) of **1**, **2**, and **3**. (a) High symmetry *k*-points in the first Brillouin zone of **1** are $\Gamma = (0, 0, 0)$, $Y = (0, 0.5, 0)$, $A = (0, 0, 0.5)$, $M = (0, 0.5, 0.5)$, $X = (0.5, 0, 0)$, $L = (0.5, 0, 0.5)$; (b) high symmetry *k*-points in the first Brillouin zone of **2** are $\Gamma = (0, 0, 0)$, $Y = (0, 0.5, 0)$, $Z = (0, 0, 0.5)$, $X = (0.5, 0, 0)$; and (c) high symmetry *k*-points in the first Brillouin zone of **3** are $Z = (0, 0.5, 0.5)$, $\Gamma = (0, 0, 0)$, $C = (0.5, 0.5, 0)$, $F = (0.5, 0.5, 0.5)$, $B = (0, 0, 0.5)$, $Y = (0.5, 0, 0)$.

the strength of π-stacking interactions in crystal **1** are weaker than those in crystal **2** and the strength of hydrogen bonding interactions are inverse. Specifically, there is 1/4 π-stacking interactions in crystal **1** whereas in crystal **2** there is 1/2. For one unit cell, there are eight intermolecular hydrogen bonds in crystal **1**, while crystal **2** has only four intermolecular hydrogen bonds, which can also be seen from the following DOS analysis. Thus, the hole mobility of crystal **2** is larger than that of crystal **1**, while the electron mobility of crystal **2** is smaller than that of crystal **1**.

As we can see from Fig. 2(c), VB of crystal **3** is almost horizontal, which means there is barely any hole transportation. However, its CB stretching along $\Gamma \rightarrow Y$ and $\Gamma \rightarrow C$ directions have larger bandwidths, which are along *a*-axis and parallel to the *ab* plane in the real space, respectively. Thus, crystal **3** can act as an electron-transport

material, which is agreement with the experimental measurement [27], formed by hydrogen bonds.

3.3. Γ point wave functions and density of states

Through analyzing band structures, we now know that **1**, **2**, and **3** are ambipolar, p-type and n-type transport materials, respectively. In addition, from comparing the directions with lager bandwidth and the directions of each interaction that we have already discussed, we become aware of that the directions of lager bandwidth and intermolecular interactions are seem to be related. In general, there is a close relationship between the charge transport and distribution of frontier molecular orbitals. The wave functions of the band-edge state at the Γ point are equivalent to the frontier molecular orbitals, namely, the HOMO for the hole and LUMO for the electron. Furthermore, the smaller DOS is, the larger bandwidth is from the viewpoint of band model. Subsequently, density of state (DOS) and Γ point wave functions of these studied compounds, which were shown in Fig. 2 (bottom) and 3, were analyzed to explain this relationship.

As it can be seen in Fig. 3, the HOMO and LUMO of **1**, **2**, and **3** are mainly localized at thiazole, thiophene and benzene rings, but rarely on trifluoromethyls. Here, the yellow color is for positive wave functions values and the blue color is for negative wave functions values. Although the wave function distributions in crystals **1** and 2 have shown some overlap between HOMO and LUMO, only about 1/4 ring in crystal 1 participates in π-stacking, and there is at least 1/2 ring in crystal 2. This also explains the larger VB of crystal **2** than crystal **1**. And as to crystal **3**, although it apparently shows great distributions of both HOMO and LUMO, there is no overlap between molecules as shown in Fig. 1, which explains the nearly flat VB.

Table 3
The percentages of the π–π interactions and the hydrogen bond in their total DOS of **1**, **2**, and **3**.

	VB		CB	
	H-bond	π–π	H-bond	π–π
1	0.097	0.562	0.090	0.416
2	0.141	0.640	0.034	0.769
3	0.804	–	0.650	–

Subsequently, we have calculated the percentages of the π–π and the hydrogen bonding interactions in their total DOS of **1**, **2**, and **3**, which is listed in Table 3. Through analyzing these percentages, it is clearly to see that the π–π interactions tend to have smaller percentage in VB than in CB, while the hydrogen bonding interactions has a smaller percentage in CB than in VB. This means that the π–π interactions has more effect on the hole transport, while the hydrogen bonding interactions has

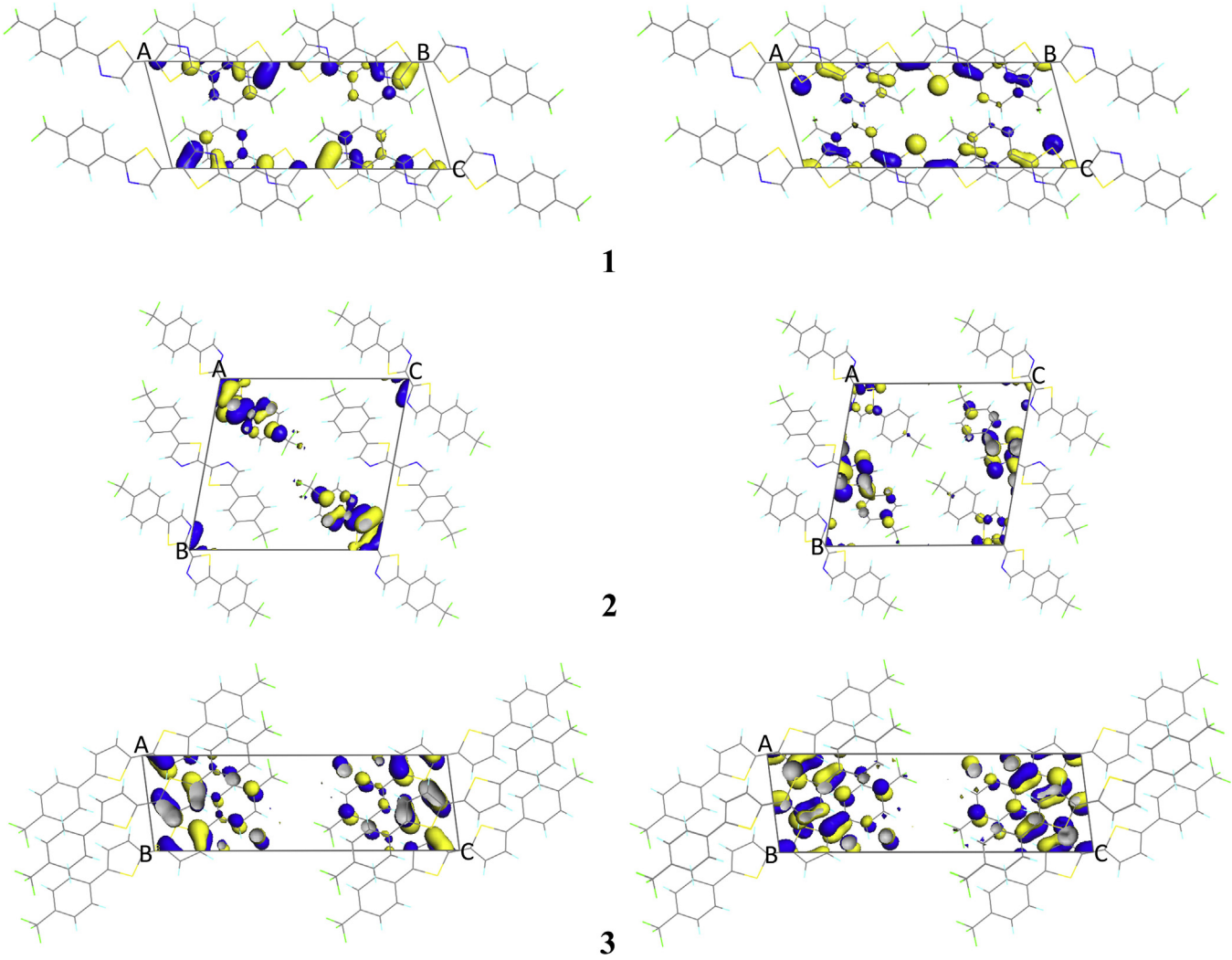

Fig. 3. Γ point wave functions of **1**, **2**, and **3**. HOMO (left), LUMO (right).

more effect on the electron transport, which is consistent with the analytic results of band structure.

4. Conclusions

In this work, we have chosen a series of thiazole/thiophene-based oligomers with trifluoromethylphenyl groups **1**, **2**, and **3** to investigate the relation between intermolecular interactions and transport properties by using band model for our studied compounds. Crystal **1** has π–π and hydrogen bonding interactions in separate directions which makes it an ambipolar transport material, while crystal **2** with π–π and hydrogen bonding interactions in the same direction acts as p-type transport material, and hydrogen bonding interactions dominated crystal **3** is n-type transport material, respectively. Thus, the π–π interactions have much effect on the hole transport, while intermolecular hydrogen bonding interactions are mainly responsible for the electron transport. These results might be favorable to further understanding the charge transport property of this kind of compounds.

Acknowledgements

The authors gratefully acknowledge the financial support from the National Natural Science Foundation of China (21273030 and 21203019), the Science and Technology Development Project Foundation of Jilin Province (20090146), The Project Sponsored by the Scientific Research Foundation for the Returned Overseas Chinese Scholars, State Education Ministry.

Appendix A. Supplementary data

Supplementary data associated with this article can be found, in the online version, at http://dx.doi.org/10.1016/j.jmgm.2014.04.016.

References

[1] M.S. Park, J.Y. Lee, Indolo acridine-based hole-transport materials for phosphorescent OLEDs with over 20% external quantum efficiency in deep blue and green, Chem. Mater. 23 (2011) 4338–4343.
[2] N. Lin, J. Qiao, L. Duan, H. Li, L. Wang, Y. Qiu, Achilles heels of phosphine oxide materials for OLEDs: chemical stability and degradation mechanism of a bipolar phosphine oxide/carbazole hybrid host material, J. Phys. Chem. C 116 (2012) 19451–19457.
[3] D.T. Chase, A.G. Fix, S.J. Kang, B.D. Rose, C.D. Weber, Y. Zhong, L.N. Zakharov, M.C. Lonergan, C. Nuckolls, M.M. Haley, 6,12-Diarylindeno[1,2-b]fluorenes: syntheses, photophysics, and ambipolar OFETs, J. Am. Chem. Soc. 134 (2012) 10349–10352.
[4] G. Generali, F. Dinelli, R. Capelli, S. Toffanin, F. di Maria, M. Gazzano, G. Barbarella, M. Muccini, Correlation among morphology, crystallinity, and charge mobility in OFETs made of quaterthiophene alkyl derivatives on a transparent substrate platform, J. Phys. Chem. C 115 (2011) 23164–23169.
[5] I. Osaka, T. Abe, M. Shimawaki, T. Koganezawa, K. Takimiya, Naphthodithiophene-based donor–acceptor polymers: versatile semiconductors for OFETs and OPVs, ACS Macro Lett. 1 (2012) 437–440.
[6] Q. Xin, S. Duhm, S. Hosoumi, N. Ueno, X.-t. Tao, S. Kera, Impact of nitrogen substitution and molecular orientation on the energy-level alignment of heteroacene films, J. Phys. Chem. C 115 (2011) 15502–15508.
[7] Y. Ie, K. Nishida, M. Karakawa, H. Tada, Y. Aso, Electron-transporting oligothiophenes containing dicyanomethylene-substituted cyclopenta[b]thiophene: chemical tuning for air stability in OFETs, J. Org. Chem. 76 (2011) 6604–6610.
[8] K. Han, J. Huang, S. Chai, S. Wen, W. Deng, Anisotropic mobilities in organic semiconductors, Nature Protocol Exchange (2013) 1070, http://dx.doi.org/10.1038/protex.2013.070.
[9] X. He, J. Borau-Garcia, A.Y. Woo, S. Trudel, T. Baumgartner, Dithieno[3,2-c:2′,3′-e]-2,7-diketophosphepin: a unique building block for multifunctional pi-conjugated materials, J. Am. Chem. Soc. 135 (2013) 1137–1147.
[10] Y. Zhan, E. Holmström, R. Lizárraga, O. Eriksson, X. Liu, F. Li, E. Carlegrim, S. Stafström, M. Fahlman, Efficient spin injection through exchange coupling at organic semiconductor/ferromagnet heterojunctions, Adv. Mater. 22 (2010) 1626–1630.
[11] Q. Meng, W. Hu, Recent progress of n-type organic semiconducting small molecules for organic field-effect transistors, Phys. Chem. Chem. Phys. 14 (2012) 14152–14164.
[12] Y. Sakamoto, S. Komatsu, T. Suzuki, Tetradecafluorosexithiophene: the first perfluorinated oligothiophene, J. Am. Chem. Soc. 123 (2001) 4643–4644.
[13] M.-H. Yoon, S.A. DiBenedetto, M.T. Russell, A. Facchetti, T.J. Marks, High-performance n-channel carbonyl-functionalized quaterthiophene semiconductors: thin-film transistor response and majority carrier type inversion via simple chemical protection/deprotection, Chem. Mater. 19 (2007) 4864–4881.
[14] M.-H. Yoon, S.A. DiBenedetto, A. Facchetti, T.J. Marks, Organic thin-film transistors based on carbonyl-functionalized quaterthiophenes: high mobility n-channel semiconductors and ambipolar transport, J. Am. Chem. Soc. 127 (2005) 1348–1349.
[15] J.A. Letizia, A. Facchetti, C.L. Stern, M.A. Ratner, T.J. Marks, High electron mobility in solution-cast and vapor-deposited phenacyl–quaterthiophene-based field-effect transistors: toward n-type polythiophenes, J. Am. Chem. Soc. 127 (2005) 13476–13477.
[16] Y. Ie, M. Nitani, M. Karakawa, H. Tada, Y. Aso, Air-stable n-type organic field-effect transistors based on carbonyl-bridged bithiazole derivatives, Adv. Funct. Mater. 20 (2010) 907–913.
[17] A. Facchetti, Y. Deng, A. Wang, Y. Koide, H. Sirringhaus, T.J. Marks, R.H. Friend, Tuning the semiconducting properties of sexithiophene by α,ω-substitution – α,ω-diperfluorohexylsexithiophene: the first n-type sexithiophene for thin-film transistors, Angew. Chem. 112 (2000) 4721–4725.
[18] Y. Ie, M. Nitani, M. Ishikawa, K.-i. Nakayama, H. Tada, T. Kaneda, Y. Aso, Electronegative oligothiophenes for n-type semiconductors: difluoromethylene-bridged bithiophene and its oligomers, Org. Lett. 9 (2007) 2115–2118.
[19] Y. Umemoto, Y. Ie, A. Saeki, S. Seki, S. Tagawa, Y. Aso, Electronegative oligothiophenes fully annelated with hexafluorocyclopentene: synthesis, properties, and intrinsic electron mobility, Org. Lett. 10 (2008) 1095–1098.
[20] Y. Ie, Y. Umemoto, T. Kaneda, Y. Aso, Electronegative oligothiophenes based on a hexafluorocyclopentene-annelated thiophene unit, Org. Lett. 8 (2006) 5381–5384.
[21] Y. Suzuki, M. Shimawaki, E. Miyazaki, I. Osaka, K. Takimiya, Quinoidal oligothiophenes with (acyl)cyanomethylene termini: synthesis, characterization, properties, and solution processed n-channel organic field-effect transistors, Chem. Mater. 23 (2010) 795–804.
[22] Y. Suzuki, E. Miyazaki, K. Takimiya, ((Alkyloxy)carbonyl)cyanomethylene-substituted thienoquinoidal compounds: a new class of soluble n-channel organic semiconductors for air-stable organic field-effect transistors, J. Am. Chem. Soc. 132 (2010) 10453–10466.
[23] S. Handa, E. Miyazaki, K. Takimiya, Y. Kunugi, Solution-processible n-channel organic field-effect transistors based on dicyanomethylene-substituted terthienoquinoid derivative, J. Am. Chem. Soc. 129 (2007) 11684–11685.
[24] B.J. Jung, N.J. Tremblay, M.-L. Yeh, H.E. Katz, Molecular design and synthetic approaches to electron-transporting organic transistor semiconductors, Chem. Mater. 23 (2010) 568–582.
[25] J. Cornil, J.L. Brédas, J. Zaumseil, H. Sirringhaus, Ambipolar transport in organic conjugated materials, Adv. Mater. 19 (2007) 1791–1799.
[26] S. Ando, R. Murakami, J.-i. Nishida, H. Tada, Y. Inoue, S. Tokito, Y. Yamashita, n-Type organic field-effect transistors with very high electron mobility based on thiazole oligomers with trifluoromethylphenyl groups, J. Am. Chem. Soc. 127 (2005) 14996–14997.
[27] S. Ando, J.-i. Nishida, H. Tada, Y. Inoue, S. Tokito, Y. Yamashita, High performance n-type organic field-effect transistors based on π-electronic systems with trifluoromethylphenyl groups, J. Am. Chem. Soc. 127 (2005) 5336–5337.
[28] L.J. Wang, Q. Peng, Q.K. Li, Z. Shuai, Roles of inter- and intramolecular vibrations and band-hopping crossover in the charge transport in naphthalene crystal, J. Chem. Phys. 127 (2007) 044506–044509.
[29] L. Wang, G. Nan, X. Yang, Q. Peng, Q. Li, Z. Shuai, Computational methods for design of organic materials with high charge mobility, Chem. Soc. Rev. 39 (2010) 423–434.
[30] M.C.R. Delgado, E.G.D.A. Kim, d.S. Filho, J.-L. Bredas, Tuning the charge-transport parameters of perylene diimide single crystals via end and/or core functionalization: a density functional theory investigation, J. Am. Chem. Soc. 132 (2010) 3375–3387.
[31] S. Salman, M.C.R. Delgado, V. Coropceanu, J.-L. Brédas, Electronic structure and charge-transport parameters of functionalized tetracene crystals: impact of partial fluorination and alkyl or alkoxy derivatization, Chem. Mater. 21 (2009) 3593–3601.
[32] R.S. Sánchez-Carrera, P. Paramonov, G.M. Day, V. Coropceanu, J.-L. Brédas, Interaction of charge carriers with lattice vibrations in oligoacene crystals from naphthalene to pentacene, J. Am. Chem. Soc. 132 (2010) 14437–14446.
[33] F. Yu, G. Yang, S. Wu, Y. Geng, Z. Su, Determination of the charge transport abilities of polymorphs [C6F5Cu]2(4,4′-bipy) with different interactions: a density functional theoretical investigation, Theor. Chem. Acc. 129 (2011)45–51.
[34] F. Yu, G. Yang, Z. Su, The effect of multiple weak interactions on the charge transport ability in polymorphs, Synth. Met. 161 (2011) 1073–1078.
[35] F. Yu, X. Tang, G. Yang, Y. Duan, Z. Su, A theoretical study of ambipolar organic transport material: 1,4-bis(pentafluorobenzyl)[60]-fullerene, Chem. Phys. Lett. 506 (2011) 255–259.
[36] N.L. Janaki, B. Priyanka, A. Thomas, K. Bhanuprakash, A computational study of semiconducting benzobisthiazoles: analysis of the substituent effects on the electronic structure, solid-state interactions, and charge transport properties using DFT methods, J. Phys. Chem. C 116 (2012) 22663–22674.
[37] M.-Q. Long, L. Tang, D. Wang, L. Wang, Z. Shuai, Theoretical predictions of size-dependent carrier mobility and polarity in graphene, J. Am. Chem. Soc. 131 (2009) 17728–17729.

[38] M.C.R. Delgado, K.R. Pigg, D.A. da Silva Filho, N.E. Gruhn, Y. Sakamoto, T. Suzuki, R.M. Osuna, J. Casado, V. Hernández, J.T.L. Navarrete, N.G. Martinelli, J. Cornil, R.S. Sánchez-Carrera, V. Coropceanu, J.-L. Brédas, Impact of perfluorination on the charge-transport parameters of oligoacene crystals, J. Am. Chem. Soc. 131 (2009) 1502–1512.
[39] R.S. Sánchez-Carrera, S.A. Odom, T.L. Kinnibrugh, T. Sajoto, E.-G. Kim, T.V. Timofeeva, S. Barlow, V. Coropceanu, S.R. Marder, J.-L. Brédas, Electronic properties of the 2,6-diiododithieno[3,2-b:2′,3′-d]thiophene molecule and crystal: a joint experimental and theoretical study, J. Phys. Chem. B 114 (2009) 749–755.
[40] J. Hafner, Ab-initio simulations of materials using VASP: density-functional theory and beyond, J. Comput. Chem. 29 (2008) 2044–2078.
[41] E.F.C. Byrd, G.E. Scuseria, C.F. Chabalowski, An ab initio study of solid nitromethane, HMX, RDX, and CL20: successes and failures of DFT, J. Phys. Chem. B 108 (2004) 13100–13106.
[42] G. Kresse, J. Hafner, Ab initio molecular dynamics for open-shell transition metals, Phys. Rev. B 48 (1993) 13115–13118.
[43] G. Kresse, J. Furthmüller, Efficient iterative schemes for ab initio total-energy calculations using a plane-wave basis set, Phys. Rev. B 54 (1996) 11169–11186.
[44] J.P. Perdew, K. Burke, M. Ernzerhof, Generalized gradient approximation made simple, Phys. Rev. Lett. 77 (1996) 3865–3868.
[45] Y. Pan, H. Zhang, D. Shi, J. Sun, S. Du, F. Liu, H.-j. Gao, Highly ordered, millimeter-scale, continuous, single-crystalline graphene monolayer formed on Ru (0 0 0 1), Adv. Mater. 21 (2009) 2777–2780.
[46] F. Yu, S.-X. Wu, Y. Geng, G.-C. Yang, Z.-M. Su, Charge transport and luminescent properties of C6F5Cu(py) and their relationships with cuprophilic interactions: a density functional theory investigation, Theor. Chem. Acc. 127 (2010) 735–742.
[47] C. Wang, H. Dong, W. Hu, Y. Liu, D. Zhu, Semiconducting π-conjugated systems in field-effect transistors: a material odyssey of organic electronics, Chem. Rev. 112 (2011) 2208–2267.